Numerical resolution of a mono-disperse model of bubble growth in magmas

Louis Forestier-Coste, Simona Mancini, Alain Burgisser, François James

Mathematical Models and Methods in Applied Sciences

A MONODISPERSE MODEL FOR WATER BUBBLES GROWTH IN MAGMAS

ALAIN BURGISSER

Institut des Sciences de la Terre d'Orléans, CNRS/INSU, Université d'Orléans, Université François Rabelais-Tours, 1A rue de la Férolerie, Orléans, F-45071 cedex 2, France
burgisse@cnrs-orleans.fr

LOUIS FORESTIER-COSTE

Laboratoire de Mathématiques - Analyse, Probabilités, Modélisation - Orléans, Fédération Denis Poisson, Université d'Orléans, CNRS/INSMI, BP. 6759, Orléans, F-45067 , France
louis.forestier-coste@math.cnrs.fr

FRANCOIS JAMES

Laboratoire de Mathématiques - Analyse, Probabilités, Modélisation - Orléans, Fédération Denis Poisson, Université d'Orléans, CNRS/INSMI, BP. 6759, Orléans, F-45067 , France
francois.james@math.cnrs.fr

SIMONA MANCINI

Laboratoire de Mathématiques - Analyse, Probabilités, Modélisation - Orléans, Fédération Denis Poisson, Université d'Orléans, CNRS/INSMI, BP. 6759, Orléans, F-45067 , France
simona.mancini@univ-orleans.fr

Received (Day Month Year)
Revised (Day Month Year)
Communicated by (xxxxxxxxxx)

Growth of gas bubbles in magmas may be modelled by a system of differential equations, accounting for radius and pressure growth, coupled with an advection-diffusion equation, defining the gas flux ingoing the bubble from magma. This system of equations is characterised by two relaxation parameters linked to the viscosity of the magma and to the diffusivity of the dissolved gas, respectively. Here, we propose a numerical scheme which, unlike previously published schemes, preserves the total mass of the coupled system of equations. We also study the asymptotic behavior of the system of equations, when letting the relaxation parameters vary from 0 to ∞, and show the numerical convergence of the solutions obtained by means of the general numerical scheme to the simplified asymptotic limits. Finally, we validate and compare our numerical results with those

obtained in experiments.

Keywords: bubble growth; mass preserving scheme; keyword3.

AMS Subject Classification: 86A04, 8608, 65L20, 65M06

1. Introduction

All volcanic eruptions involve a decompression of the magma during its ascent from the Earth's crust to the surface. This decompression causes the volatiles dissolved into the magma to come out of solution as gas bubbles. The way these bubbles are growing, whether they coalesce with one another or travel faster than or with the magma, are all conditioning the way the volcanic eruption will unfold. Bubbles that remain trapped with the magma they originally grew from will accumulate gas pressure until failure of the magma releases it suddenly to produce an explosive eruption. Such scenario is most likely when the magma is highly viscous and prevails bubble motion. This situation is propitious to modelling because bubbles can be considered as immobile in the magma and the resulting spherical geometry allows one to reduce bubble growth to a system of differential equations describing the evolution of pressure and gas mass in a bubble coupled with an advection-diffusion equation describing the drainage of the dissolved gas towards the bubble. A further assumption is that bubbles are exclusively made of water vapour, which can be justified by the fact that water is, by far, the most abundant volatile species in such viscous magmas.

Since the seminal work done in Scriven,[15] several numerical schemes that solve such system of differential equations have been proposed (see Ref 1, 17, 18, 3, 14). Application to gas bubble in magmas is slightly more recent (see Ref. 13, 12, 16, 4, 11, 5). All these schemes have in common a discretization of the advection-diffusion equation that is not strictly conservative with respect to the diffused species. They also involve user-defined discretization parameters that have to be empirically adjusted to ensure sufficient convergence and/or accuracy of the scheme. Developing alternate, robust schemes would allow including the dynamics of bubble growth into more sophisticated model that take into account, for instance, that bubble have different sizes, or that, if magma viscosity is low enough, bubble may rise with respect to the magma.

The present work is developed as follows. In section 2, we recall the differential equations describing the respective evolution of bubble radius and mass, together with the advection-diffusion equation concerning the behavior of the water concentration in the magma. Following Lensky *et al.*,[11] we write the problem in dimensionless form, introducing two relaxation parameters Θ_V and Θ_D. Section 3, is devoted to the numerical approximation of the model. The main novelty is the discretization of the advection-diffusion equation, see 3.2, in which we explain how to compute the

mesh and flux at each iteration. In section 4 we deal with the asymptotic of the dimensionless problem, when the rate between the relaxation parameters varies from 0 to ∞. Three main regimes are underlined: viscous, diffusive, and equilibrium. For each limit, we also propose a way to discretize it. Numerical results, the convergence of the solution towards the simplified asymptotic limits, and the comparison with experiments are discussed in section 5. Finally, in section 6, we summarise our study and suggest possible extensions of the modelling of bubbles growth in magma.

2. The model

We are interested in the modelling of bubble growth in a highly viscous magma. This has two main consequences on the model. The first one is that we assume that bubbles do not interact with each other, in particular there are no coalescence effects. This is strongly limitative for the simulation of a magmatic conduit, but this phenomenon can be controlled in some laboratory experiments, see section 5.2. The other point is that, due to the high viscosity of the magma, bubbles travel along with the same velocity, namely the one of the melt. In other words, they can be considered as immobile with respect to the melt.

At this stage, we can consider that a bubble can be described with two parameters, its volume $\hat{V}$ and its gaseous mass $\hat{M}$. Taking into account that the bubble is made only of water in gaseous form, we can write the perfect gases law inside the bubble, in order to introduce the gas pressure $\hat{P}$, and the gas density $\hat{\rho}$:

$$GT\hat{\rho} = \hat{P}M_w, \tag{2.1}$$

with M_w the molar mass for water, G the perfect gas constant and T the gas temperature, which is assumed to be constant during the process. Next, following Lensky *et al.*,[11] we assume that the bubble is spherical, with radius $\hat{R}$, so that $\hat{V} = \frac{4}{3}\pi\hat{R}^3$, and we set for future convenience $\hat{M} = \hat{\rho}\hat{R}^3$, so that the bubble mass is $\frac{4}{3}\pi\hat{M}$. Thus we can choose the radius $\hat{R} = \hat{R}(t)$ and the variable $\hat{M} = \hat{M}(t)$, proportional to the mass, to describe the evolution of the bubble, and seek for a system of differential equations for these variables. Notice that in Lensky *et al.*[11] an equation on the pressure $\hat{P}(t)$ is given, we choose here to write things in terms of mass, because it leads to a better handling of the mass conservation at numerical level. Such a model gives a description of the growth of a single bubble, or for a population of identical, non-interacting bubbles: this is the so-called mono-disperse case.

2.1. *Basic equations*

First we briefly recall the origin of the equations. Two main physical processes drive the bubble growth, both originating from the magma decompression as it moves towards the surface. On the one hand, the gas trapped into the bubble is expanding; on the other hand, the water dissolved in the magma is diffusing and

eventually is vaporized in the bubble, so that the water concentration profile in the melt has to be considered as well.

The equations describing the time evolution for the bubble radius and pressure and for the water concentration have been described in the literature several times. Therefore, we shall not reproduce here this derivation and, for example, we refer the reader to the works of Arefmanesh *et al.*[1], L'Heureux,[8] Proussevitch *et al.*[13] and Scriven.[15] We recall briefly the origin of each equation, and their coupling.

The growth of the bubble in the magma involves the ambient pressure in the magma $\hat{P}_a(\hat{t})$, which is a given function of time, viscous effects and surface tension effects. A convenient model for $\hat{P}_a$, quite simple and compatible with experimental conditions, is a linear decrease from an initial value P_i at constant decompression rate ΔP:

$$\hat{P}_a(\hat{t}) = P_i - \hat{t}\Delta P. \tag{2.2}$$

From the momentum conservation of Navier-Stokes equations, neglecting the inertial terms, and considering incompressibility of the fluid one obtains

$$\hat{P}(\hat{t}) - \hat{P}_a(\hat{t}) = \frac{2\sigma}{\hat{R}(\hat{t})} + 4\frac{\dot{\hat{R}}(\hat{t})}{\hat{R}(\hat{t})}\hat{\eta},$$

where σ is the surface tension, $\hat{\eta}$ is the magma viscosity, both parameters which are assumed constant in this paper. We rewrite this as a differential equation on the radius $\hat{R}$:

$$\dot{\hat{R}}(\hat{t}) = \frac{\hat{R}(\hat{t})}{4\hat{\eta}}\left(\hat{P}(\hat{t}) - \hat{P}_a(\hat{t}) - \frac{2\sigma}{\hat{R}(\hat{t})}\right). \tag{2.3}$$

To obtain the inside pressure $\hat{P}(\hat{t})$, or equivalently by (2.1) the gaseous water mass $\hat{M}(\hat{t})$, we need to study the mass conservation of water. First we consider the volatile mass balance at the bubble-magma interface, which writes in spherical geometry

$$\frac{4\pi}{3}\frac{d}{d\hat{t}}\left(\hat{\rho}\hat{R}^3\right) = 4\pi\hat{\rho}_m F_{\hat{R}(\hat{t})}, \tag{2.4}$$

where $F_{\hat{R}(\hat{t})}$ represents the water flux from the magma into the bubble at the interface. It is estimated by the global water mass balance between the bubble and its surroundings. At this stage, we introduce the concentration of water in the melt, which is a function $C = C(\hat{r}, \hat{t})$ of the time $\hat{t}$ and on the radial distance from the boundary of the bubble, $\hat{r} \in [\hat{R}(\hat{t}), \hat{S}(\hat{t})]$. With this notation, the flux $F = F(\hat{r}, \hat{t})$ in equation (2.4) is given by

$$F_{\hat{R}(\hat{t})} = \hat{D}\hat{R}^2 \left.\frac{\partial C}{\partial \hat{r}}\right|_{\hat{r}=\hat{R}(\hat{t})}. \tag{2.5}$$

More precisely, we assume that the bubble has influence only on a finite region surrounding it. This region is called the influence region, and it is quite natural for a spherical bubble to assume that it is a sphere of radius $\hat{S} = \hat{S}(t)$ and centre

the bubble centre. The evolution of $\hat{S}$ is obtained under the assumption that the volume of the influence region is constant in time (see Ref. 11), so that

$$\hat{S}(\hat{t}) = \left(\hat{S}_0^3 + \hat{R}(\hat{t})^3\right)^{1/3}, \tag{2.6}$$

where $\hat{S}_0$ is a constant representing the radius of the influence region when the bubble has a null radius $\hat{R}$.

The definition of the influence region implies that the total water mass inside it, that is the sum of the water mass in the bubble and of the water dissolved in its influence region, must remain constant in time. Assuming that for a bubble of radius zero the water concentration in magma is a constant C_0, this may be expressed in the following form:

$$\frac{4\pi\hat{\rho}(\hat{t})}{3}\hat{R}^3(\hat{t}) + 4\pi\hat{\rho}_m \int_{\hat{R}(\hat{t})}^{\hat{S}(\hat{t})} \hat{r}^2 C(\hat{r},\hat{t})\, d\hat{r} = \frac{4\pi\hat{\rho}_m}{3}\hat{S}_0^3 C_0, \tag{2.7}$$

where $\hat{\rho}$ and $\hat{\rho}_m$ are respectively the density of the gas and the magma.

Within the the influence region, that is for radii $\hat{r} \in]\hat{R}(\hat{t}), \hat{S}(\hat{t})[$, the water concentration is assumed to follow an advection-diffusion equation

$$\frac{\partial C}{\partial \hat{t}} + v_m \frac{\partial C}{\partial \hat{r}} = \frac{1}{\hat{r}^2}\frac{\partial}{\partial \hat{r}}\left(\hat{r}^2 \hat{D}\frac{\partial C}{\partial \hat{r}}\right),$$

where $\hat{D}$ is the magma diffusion coefficient, assumed constant in this work, and v_m is the radial velocity in the melt. The latter is obtained by solving the continuity equation in radial form and considering the incompressibility of the melt (see Ref. 15). Therefore v_m is given by

$$v_m = \dot{\hat{R}}\frac{\hat{R}^2}{\hat{r}^2}.$$

The advection-diffusion finally reads

$$\frac{\partial C}{\partial \hat{t}} + \dot{\hat{R}}\frac{\hat{R}^2}{\hat{r}^2}\frac{\partial C}{\partial \hat{r}} = \frac{1}{\hat{r}^2}\frac{\partial}{\partial \hat{r}}\left(\hat{r}^2 \hat{D}\frac{\partial C}{\partial \hat{r}}\right), \tag{2.8}$$

and has to be complemented with boundary conditions. On the one hand, for $\hat{r} = \hat{R}$, that is at the bubble-melt interface, the pressure has to be in equilibrium with water concentration, following Henry's law

$$C(\hat{R},\hat{t}) = K_H\sqrt{\hat{P}}, \quad \text{where } K_H \text{ is the Henry constant.} \tag{2.9}$$

The other boundary condition is given at the external interface of the influence region, and follows from the global mass balance (2.7). Indeed, stating that the time derivative of (2.7) has to be zero, a straightforward computation taking into account (2.8) and (2.4) shows that the water flux on the outer border of the influence region, $\hat{r} = \hat{S}$, is null:

$$\left.\frac{\partial C}{\partial \hat{r}}\right|_{\hat{r}=\hat{S}} = 0, \tag{2.10}$$

Finally, we are lead to the following system of differential equations

$$\begin{aligned} \dot{\hat{R}}(\hat{t}) &= \frac{\hat{R}(\hat{t})}{4\hat{\eta}} \left(\hat{P}(\hat{t}) - \hat{P}_a(\hat{t}) - \frac{2\sigma}{\hat{R}(\hat{t})} \right), \\ \dot{\hat{M}}(\hat{t}) &= 3\hat{\rho}_m \hat{D} \hat{R}^2 \left. \frac{\partial C}{\partial \hat{r}} \right|_{\hat{r}=\hat{R}(\hat{t})}, \end{aligned} \tag{2.11}$$

where C solves the advection-diffusion equation (2.8), with boundary conditions (2.9) and (2.10).

An important physical quantity in this context is the porosity, or void fraction, of the magma. Porosity is actually a macroscopic notion, as far as it can be given a meaning for a single bubble, we choose, following Lensky *et al.* [11], to define it as

$$\alpha = \frac{\hat{R}(\hat{t})^3}{\hat{S}(\hat{t})^3}.$$

All the simulations performed in this paper tend to compute a porosity as close as possible to 1, even if it is not realistic from a physical viewpoint: the crossover value where a model of bubbles in a melt is no longer valid is around 0.7.

2.2. *Dimensionless problem*

In the model we obtained, the physical parameters involved may vary for several orders of magnitude and in a very intricate manner. Table 1 recalls their meaning and presents a sample of these values, which come from the experimental results quoted below.

Table 1. Physics constants values

D	diffusivity	10^{-12} $(m^2 \cdot s^{-1})$
$\hat{\eta}$	viscosity	10^4 $(Pa \cdot s)$
M_w	molar mass for water	18.10^{-3} $(kg \cdot mol^{-1})$
G	perfect gases constant	8.3144 $(J \cdot mol^{-1} \cdot K^{-1})$
T	temperature	1098.15 (K)
σ	surface tension	0.1 $(J \cdot m^{-2})$
ρ_m	magma density	2154 $(kg \cdot m^{-3})$
K_H	Henry constant	$3.44.10^{-6}$ $(kg^{-1/2} \cdot m^{1/2})$
S_0	influence radius for $R = 0$	$6.204.10^{-5}$ (m)
ΔP	decompression rate	10^5 $(Pa \cdot s^{-1})$
P_i	initial ambient pressure	10^8 (Pa)
C_0	water concentration for $R = 0$	4.21 $(wt.\%)$

The behaviour of the solutions to the model can vary drastically with these values, from one experimental situation to another, but also during a single experiment. The aim of this section is to provide a dimensionless set of equations, in order to identify more easily several specific regimes.

To do this, we need to define a set of "characteristic dimensions" for the system. Then a convenient scaling of the parameters and variables will lead to the desired dimensionless equations. Following Lensky *et al.*,[11] it turns out that a set of five dimensions gives a physically relevant scaling, namely a bubble radius, a pressure, a density, a viscosity coefficient and a diffusion coefficient. These characteristic dimensions are chosen here as the corresponding initial values: the initial bubble radius, R_i, the initial gas density ρ_i, the initial ambient pressure $P_i = P_a(t=0)$ and the diffusion and viscosity coefficients, D_i and η_i. Then we perform the following scalings on variables and parameters:

$$\eta = \frac{\hat{\eta}}{\eta_i} \qquad D = \frac{\hat{D}}{D_i} \qquad \rho_m = \frac{\hat{\rho}_m}{\rho_i} \qquad \Sigma = \frac{2\sigma}{R_i P_i}$$

$$R = \frac{\hat{R}}{R_i} \qquad S = \frac{\hat{S}}{R_i} \qquad r = \frac{\hat{r}}{R_i} \qquad \dot{R} = \frac{\dot{\hat{R}} P_i}{R_i \Delta P}$$

$$P = \frac{\hat{P}}{P_i} \qquad P_a = \frac{\hat{P}_a}{P_i} \qquad \rho = \frac{\hat{\rho}}{\rho_i} \qquad t = \hat{t}\frac{\Delta P}{P_i}$$

We note that, since the diffusion and viscosity coefficients are considered to be constant, we have that $D \equiv 1$ and $\eta \equiv 1$. In the same way, equations (2.2) and (2.6) become respectively

$$P_a = 1 - t \tag{2.12}$$

and

$$S^3(t) = S_0^3 + R^3(t). \tag{2.13}$$

Finally, we set $M = \rho R^3$ in the following.

Straightforward computations show that the mass conservation equation (2.7) becomes

$$M + 3\rho_m \int_{R(t)}^{S(t)} r^2 C \, dr = S_0^3 \, C_0 \rho_m, \tag{2.14}$$

and the system of differential equations on mass and radius (2.11) rewrites

$$\dot{R} = \frac{R}{\Theta_V}\left(P - P_a - \frac{\Sigma}{R}\right), \tag{2.15}$$

$$\dot{M} = \frac{3\rho_m}{\Theta_D}\left(r^2 \frac{\partial C}{\partial r}\right)_{r=R}, \tag{2.16}$$

where we have introduced the relaxation parameters:

$$\Theta_V = \frac{4\eta_i \Delta P}{P_i^2}, \qquad \Theta_D = \frac{R_i^2 \Delta P}{D_i P_i}. \tag{2.17}$$

Finally, the water concentration in the melt satisfies the dimensionless advection-diffusion equation

$$\partial_t C + \frac{\dot{R}R^2}{r^2}\partial_r C = \frac{1}{\Theta_D}\frac{1}{r^2}\partial_r\left(r^2\partial_r C\right) \tag{2.18}$$

with the following boundary conditions:

$$C(R,t) = C_i\sqrt{P}, \qquad \left.\frac{\partial C}{\partial r}\right|_{r=S} = 0, \tag{2.19}$$

where C_i is given by $C_i = K_H\sqrt{P_i}$.

It is clear now that the parameters Θ_D and Θ_V defined by (2.17) are driving the behaviour of all the equations involved, and will be referred to as the viscosity Θ_V and diffusion Θ_D relaxation parameters, since they are dimensionless. Their extreme values define several specific regimes which are analyzed in section 4 below.

At this stage, it is worth to state the initial conditions in some details. From the above normalization process, the initial radius is $R = 1$, and the corresponding initial pressure is assumed to be at equilibrium with the ambient pressure and the surface tension:

$$P(0) = (P_a(0) + \Sigma)/\Theta_V.$$

We need also to specify the initial water concentration in the influence region, that is $C(0,r)$ for $r \in [R(0), S(0)]$. Usually, we choose $C(0,r) = C_0$, where C_0 is a positive constant.

It turns out that the behaviour of the solutions drastically depends on the relationships between the initial concentration and the initial bubble pressure. A particular regime is given by

$$C(0,r) \equiv C_0 = C_i\sqrt{P(0)}, \quad r \in [R(0), S(0)]. \tag{2.20}$$

These "well-prepared" initial data correspond physically to some equilibrium between the inner bubble pressure and the water concentration. The solution behaves nicely as expected: the radius increases, the inner pressure decreases. On the other hand, when (2.20) is not satisfied, one can observe some kind of initial layer for small times (depending on the value of Θ_V), where bubble pressure and water concentration try to reach equilibrium. If $C_0 > C_i\sqrt{P(0)}$, there is a water excess in the melt, so that the radius may decrease or the pressure increase very fast before reaching a smooth regime. On the contrary, the water deficit $C_0 < C_i\sqrt{P(0)}$ tends to limit or prevent nucleation of bubbles, and the solution may exhibit almost discontinuous behaviour, or even not exist.

3. Numerical approximation

In this section we consider the numerical approximation of the model (2.15)-(2.16)-(2.18), on $R(t)$ and $M(t)$ and $C(r,t)$, together with the boundary conditions (2.19) and the external assumption (2.12)-(2.13). In particular, we propose a numerical

scheme for the advection-diffusion equation conserving the water mass. This is a delicate point of the discretisation; the flux at the bubble border has to be carefully computed because the magnitude of the relaxation parameters Θ_V and Θ_D may differs of several orders. We shall first present the straightforward discretization of the system of differential equations (2.15)-(2.16) and follow by presenting the more critical problem of the advection-diffusion equation, (2.18), discretization.

3.1. *The differential system*

We describe here the basic elements of the numerical scheme for the differential system (2.15)-(2.16).

Let us first define, for $n \in \mathbb{N}$, the time t^{n+1} and the ambient pressure $P_a^{n+1} = P_a(t^{n+1})$, at the iteration step $n+1$, respectively by:

$$t^{n+1} = t^n + \Delta t^n,$$

$$P_a^{n+1} = 1 - t^{n+1},$$

where the time step Δt^n is computed at each iteration and must satisfy some stability conditions which will specified later on, see section 3.3. The numerical results, see section 5, will be plotted in term of the ambient pressure P_a, which may be considered as a time variable.

We choose a semi-implicit scheme for the discretisation of (2.15), in the sense that the discrete bubble radius $R^n = R(t^n)$ is treated implicitly, whereas the pressure $P^n = P(t^n)$ remains explicit. Thus the evolution of the discrete radius is given by

$$R^{n+1} = \left(R^n - \Delta t^n \frac{\Sigma}{\Theta_V}\right)\left(1 - \Delta t^n \frac{(P^n - P_a^n)}{\Theta_V}\right)^{-1}. \tag{3.1}$$

Next we discretize the equation for the mass balance at the magma-bubble interface, (2.16), by a semi-explicit scheme. Defining the discrete bubble mass by $M^n = M(t^n)$, we recall that the pressure is given for all n by $P^n(R^n)^3 = M^n$. We denote by $F_0^n = F(R, t^n)$ the discrete flux at the interface $r = R$, and we set

$$M^{n+1} = M^n + 3\rho_m \frac{\Delta t^n}{\Theta_D} F_0^{n+1}. \tag{3.2}$$

Finally, the discrete radius of the influence region, $S^n = S(t^n)$ is given by $S^n = \left((R^n)^3 + S_0^3\right)^{1/3}$.

We turn now to the definition of the discrete flux F_0^{n+1}, which follows from the discretization of the advection-diffusion equation (2.18).

3.2. *The advection-diffusion discretization*

The advection-diffusion equation for the water concentration $C(t, r)$ is solved by splitting the equation between the advection step and the diffusion step.

The advection step consists in discretizing the following transport equation:

$$r^2\partial_t C + \dot{R}R^2\partial_r C = 0. \tag{3.3}$$

We choose to solve it by a Lagrangian method, namely, a set of mesh points at time t^n being given, r_i^n, $0 \leq i \leq N$, we compute a new mesh at time t^{n+1} by solving explicitly the equation of characteristics

$$r_i^2 \frac{dr_i}{dt} = R^2\dot{R}, \tag{3.4}$$

which integrates in

$$r_i^{n+1} = \left(\left(R^{n+1}\right)^3 - \left(R^n\right)^3 + \left(r_i^n\right)^3\right)^{1/3}. \tag{3.5}$$

The above relation defines the mesh for all $n \geq 1$ as soon as the initial discretization r_i^0, $0 \leq i \leq N$, is fixed. It is clear on this formula that, provided $r_0^0 = R^0$ and $r_N^0 = S^0$, we have for all $n \geq 1$ $r_0^n = R^n$ and $r_N^n = S^n$, so that any choice $R^0 < r_0^0 < \cdots < r_{n-1}^0 < S^0$ is relevant, in particular the uniform grid defined by $r_i^0 = \left(\frac{i}{N}S_0^3\right)^{1/3}$. Finally, we denote by Δr_i^n the (non uniform) space discretization step, $\Delta r_i^n = r_{i+1}^n - r_i^n$.

The diffusion step consists in discretizing the equation

$$r^2 d_t C = \frac{1}{\Theta_D}\partial_r\left(r^2\partial_r C\right).$$

Following a standard finite volume strategy, we integrate the above equation on the mesh $[t^n, t^{n+1}[\times]r_i^{n+1}, r_{i+1}^{n+1}[$, looking for piecewise constant solutions C_i^n on the mesh. We obtain, for $i = 1, ..., N-1$:

$$C_i^{n+1} = C_i^n + \frac{\Delta t^n}{\Theta_D}\frac{3\left(F_{i+1}^{n+1} - F_i^{n+1}\right)}{r_{i+1}^3 - r_i^3}, \tag{3.6}$$

where F_i^{n+1} stands for the discrete flux between cells $i-1$ and i for $i = 1, ..., N-1$. As an approximation of $r^2\partial_r C$ for $r = r_i^{n+1}$, we choose a centered finite difference:

$$F_i^{n+1} = \frac{2\left(r_i^{n+1}\right)^2}{r_{i+1}^{n+1} - r_{i-1}^{n+1}}\left(C_i^n - C_{i-1}^n\right). \tag{3.7}$$

The boundary conditions (2.19) become

$$C_0^{n+1} = K_H\sqrt{P_i\,P^n}, \qquad F_N^{n+1} = 0. \tag{3.8}$$

We are now in position to close equation (3.2) by setting the value of the discrete flux at the bubble-magma interface, F_0^{n+1}. The trick here is to obtain a discrete analogue of the mass preservation (2.14). Defining the discrete total water mass $\mathcal{M}^n$ by

$$\mathcal{M}^n = M^n + \rho_m\sum_{i=0}^{N-1} C_i^n\left(r_{i+1}^3 - r_i^3\right), \tag{3.9}$$

we have the following result.

Proposition 3.1. *Let F_0^{n+1} be given by*

$$F_0^{n+1} = F_1^{n+1} - \frac{\Theta_D}{\Delta t^n}\frac{r_1^3 - r_0^3}{3}(C_0^{n+1} - C_0^n). \tag{3.10}$$

Then the numerical scheme (3.1)-(3.10) *conserves the discrete total water mass, that is* $\mathcal{M}^n = \mathcal{M}^0, \quad \forall n \in \mathbb{N}$.

Proof. The total water mass at time t^{n+1} is equal to:

$$\mathcal{M}^{n+1} = M^{n+1} + \rho_m \sum_{i=0}^{N-1} C_i^{n+1}\left(r_{i+1}^3 - r_i^3\right).$$

Applying (3.2), splitting the sum for $i = 0$ and $i = 1...N-1$ and replacing (3.6) in the sum, we obtain:

$$\mathcal{M}^{n+1} = M^n + 3\rho_m\frac{\Delta t^n}{\Theta_D}F_0^{n+1} + \rho_m C_0^{n+1}(r_1^3 - r_0^3) +$$

$$+\rho_m \sum_{i=1}^{N-1} C_i^n(r_{i+1}^3 - r_i^3) + 3\rho_m\frac{\Delta t^n}{\Theta_D}\sum_{i=1}^{N-1}\left(F_{i+1}^{n+1} - F_i^{n+1}\right).$$

Hence, simplifying the last sum we get:

$$\mathcal{M}^{n+1} = M^n + 3\rho_m\frac{\Delta t^n}{\Theta_D}F_0^{n+1} + \rho_m C_0^{n+1}(r_1^3 - r_0^3) +$$

$$+\rho_m \sum_{i=1}^{N-1} C_i^n(r_{i+1}^3 - r_i^3) + 3\rho_m\frac{\Delta t^n}{\Theta_D}(F_N^{n+1} - F_1^{n+1}).$$

Recalling that $F_N^n = 0$ for all n, and splitting, in the definition $\mathcal{M}^n$, the sum for $i = 0$ and $i = 1...N-1$, we must have that:

$$3\rho_m\frac{\Delta t^n}{\Theta_D}F_0^{n+1} + \rho_m C_0^{n+1}(r_1^3 - r_0^3) - 3\rho_m\frac{\Delta t^n}{\Theta_D}F_1^{n+1} = \rho_m C_0^{n+1}(r_1^3 - r_0^3),$$

which is verified since F_0^{n+1} is defined by (3.10). □

Remark 3.1. Notice that Proposition 3.1 holds true for any choice of the discrete flux in (3.7) for $1 \le i \le N-1$.

3.3. *Stability conditions*

In this section, we describe how to compute for each $n \ge 1$ a time step Δt^n ensuring some stability conditions on the numerical approximations. The idea is to compute a bound for Δt^n for each numerical approximation (radius, mass, concentration), and then to take Δt^n the minimum of the three stability conditions.

Before dealing with equations (3.1) and (3.6), we notice that we cannot obtain a completely satisfactory stability condition for the bubble mass approximation (3.2).

However, a partial condition is given by asking that the discrete bubble pressure P^n remains larger than the ambient pressure P_a^n at each iteration n. This leads to

$$\Delta t^n < \Theta_V \left| \frac{|(P_a^n - P^n)(R^3)^n - 3\rho_m(r_1^3 - r_0^3)C_0^n|}{|3\rho_m F_1^n|} \right| \tag{3.11}$$

This condition permits in almost all cases to compute reasonable time steps, namely $\Delta t^n \sim 10^{-9}$ with respect to 10^{-12} when both Θ_V and Θ_D are small. It is not sufficient to avoid oscillations in the solution, in particular when the initial conditions are not well prepared in the sense given above, see equation (2.20). Nevertheless the scheme is robust in the sense that these oscillations, which appear at the beginning of the computation, tend to disappear when time increases. In some rare case, the oscillations blow up, but this is consistent with the physical incompatibility invoked above.

We look now for the stability conditions of (3.1) and (3.6). In particular we search a bound of the time step Δt^n such that each solution is positive.

Proposition 3.2. *Assume that for* $n \in \mathbb{N}$

$$\Delta t^n < \min\left(\frac{R^n \Theta_V}{\Sigma}, \frac{\Theta_V}{|P^n - P_a^n|} \right). \tag{3.12}$$

Then the solution to the numerical scheme (3.1) *is positive, i.e.* $R^n > 0$.

Proof. Let us assume that at the iteration n all the variables are positive, then at the iteration $n+1$, using (3.1), Δt^n must be such that:

$$\left(R^n - \Delta t^n \frac{\Sigma}{\Theta_V} \right) \left(1 - \Delta t^n \frac{P^n - P_a^n}{\Theta_V} \right)^{-1} > 0.$$

We have two possibilities. The first one is when $P^n - P_a^n \leq 0$. Then we have:

$$1 - \Delta t^n \frac{P^n - P_a^n}{\Theta_V} > 0.$$

Hence,

$$R^n - \Delta t^n \frac{\Sigma}{\Theta_V} > 0$$

which implies,

$$\Delta t^n < \frac{\Theta_V R^n}{\Sigma}.$$

The second one is: $P^n - P_a^n > 0$. Then Δt^n must be the positive solution of a second order equation with a positive dominant coefficient:

$$\frac{\Sigma(P^n - P_a^n)}{\Theta_V^2}.$$

Hence R^{n+1} is positive, if Δt^n is external to the roots:

$$\frac{\Theta_V}{P^n - P_a^n}\,, \quad \frac{R^n \Theta_V}{\Sigma}.$$

Finally, we remark that the choice (3.12) verifies both conditions. □

Proposition 3.3. *Assume that, for* $n \in \mathbb{N}$,

$$\Delta t^n < \frac{\Theta_D}{6} \min_i \left((r_{i+1}^3 - r_i^3) \left(\frac{r_{i+1}^{n+1} - r_{i-1}^{n+1}}{(r_i^{n+1})^2} \right) \right). \tag{3.13}$$

Then the solution to the numerical scheme (3.6) *is positive, i.e.* $C_i^n > 0$ *for all* $i = 1, \ldots, N-1$.

Proof. We first remark that the Dirichlet condition on the boundary $r = R$ implies that $C_0^n > 0$ for all $n \in \mathbb{N}$.
Assuming that at the n^{th} iteration C_i^n is positive for all $i = 0...N-1$, we want Δt^n to verify $C_i^{n+1} > 0$. Thus from (3.6), it must be, for $i = 1...N-1$:

$$C_i^n + \frac{3\Delta t^n}{\Theta_D (r_{i+1}^3 - r_i^3)} \left(F_{i+1}^{n+1} - F_i^{n+1} \right) > 0.$$

Recalling that F_i^{n+1} is given by (3.7), collecting the terms with respect to C_{i-1}^n, C_i^n and C_{i+1}^n and considering that C_i^n are positive for all i, we get a sufficient condition for the positivity of C_i^{n+1} in the form, for $i = 1...N-2$:

$$1 - \frac{6\Delta t^n}{\Theta_D (r_{i+1}^3 - r_i^3)} \left(\frac{(r_{i+1}^{n+1})^2}{r_{i+2}^{n+1} - r_i^{n+1}} + \frac{(r_i^{n+1})^2}{r_{i+1}^{n+1} - r_{i-1}^{n+1}} \right) > 0.$$

Since

$$\frac{r_{i+2}^{n+1} - r_i^{n+1}}{(r_{i+1}^{n+1})^2} > 0,$$

the time step Δt^n given by (3.13) verifies the above condition.
If now $i = N-1$, recalling that $F_N^n = 0$ for all n, we obtain that Δt^n must satisfy:

$$\Delta t^n < \frac{\Theta_D}{6} (r_N^3 - r_{N-1}^3) \left(\frac{r_N^{n+1} - r_{N-2}^{n+1}}{(r_{N-1}^{n+1})^2} \right)$$

which conclude the proof. □

4. Limit cases

As mentioned in section 2, the system of equation (2.15)-(2.16)-(2.18) we are considering, has two relaxation times, Θ_V and Θ_D defined by (2.17), which may differ by several order of magnitude, depending on the values of, for instance, diffusivity or viscosity. In many experiments Θ_V and/or Θ_D are very small, of the order of 10^{-7}. The time steps Δt^n depending on these values, the computational time needed

to reach a porosity close to 1 is very large. The study of the limit cases, such as when Θ_V and Θ_D tends to ∞ or to 0, is thus an attractive alternative to solving the full system because it leads to simplified models with smaller simulation times. In particular, we will classify the different limits in regimes of bubble growth by considering the ratio Θ_V/Θ_D. Following Lensky *et al.*,[11], we define a viscous regime when the ratio is very small, see 4.1, an equilibrium regime when the ratio is of order 1, see 4.2, and a diffusive regime when the ratio is large, see 4.3. At the end of each section, we will also summarise when necessary the numerical scheme corresponding to the simplified cases. As we are mainly interested in the behavior of the bubble physical dimensions (pressure P and radius R), we shall only describe how to compute these two quantities. In particular, we recall that, when comparing with experiments, we consider the porosity: $\alpha = R^3/S^3$. We list all the possible limits in table 2, which references each simplification to compute the bubble radius R and mass M (or pressure P). In table 2 we also give the orders of magnitude delimiting each regime.

Table 2. Limit cases

Θ_D \ Θ_V	0	10^{-5}	10^{1}	∞
∞	4.1.2 (4.4), (4.2)	4.1.1 (4.3), (4.2)	4.2.2 (4.12), (4.2)	
10^{3}	4.1.3 (4.5), (4.6)	(2.15), (2.16)	4.3.1 (4.12),(4.13)	
10^{-3}	4.2.1 (4.5), (4.9)	4.3.3 (4.9), (2.15)	4.3.2 (4.12), (4.14)	

4.1. *Viscous regime :* $\Theta_V/\Theta_D << 1$

We first look at the case when the viscous relaxation parameter is smaller than the diffusion one. There are three possibilities: Θ_V goes to zero and Θ_D is of order 1 or goes to infinity; and Θ_V is of order 1 and Θ_D goes to infinity.

4.1.1. $\Theta_V \sim 1$ *and* $\Theta_D \to \infty$

Since Θ_D is very large, equation (2.18) reads $r^2 d_t C(r,t) = 0$, which yields to:

$$\int_{R(t)}^{S(t)} r^2 C(r,t)\, dr = \int_{R(0)}^{S(0)} r^2 C_0\, dr. \tag{4.1}$$

Concerning the bubble mass evolution, since $\Theta_D >> 1$, equation (2.16) reads $\dot{M} = 0$, which is equivalent to:

$$M = M(0), \tag{4.2}$$

the water mass inside the bubble is constant. In fact, a large diffusive relaxation parameter may be physically given by a very small value for the diffusivity in magma; hence there will not be diffusion of water from the magma into the bubble, and the bubble water mass will not change.

As $\Theta_V \sim 1$, no simplification is possible for the equation giving the evolution of the bubble radius (2.15). Still, recalling that $M(0) = M = PR^3$ and that the ambient pressure is given by (2.12), we can write a differential equation only depending on R:

$$\dot{R} = \frac{1}{\Theta_V}\left(\frac{M(0)}{R^2} - R(1-t) - \Sigma\right), \tag{4.3}$$

or equivalently on P:

$$\dot{P} = -\frac{3P}{\Theta_V}\left(P - (1-t) - \Sigma\left(\frac{P}{M(0)}\right)^{1/3}\right).$$

We note that we obtain the same result as in Ref. 11. Equation (4.3) can be easily solved with an implicit scheme.

4.1.2. $\Theta_V \to 0$ *and* $\Theta_D \to \infty$

When Θ_D is large, the simplifications (4.1) and (4.2) are always true. In particular, water mass in the bubble is constant: $M = M(0)$.

Regarding equation (2.15), since Θ_V is very small, multiplying by Θ_V, recalling that $M(0) = PR^3$, and simplifying allows us to obtain a third order equation on R:

$$R^3(1-t) + \Sigma R^2 - P(0) = 0,$$

which admits an unique real solution given by the explicit relation

$$R = \frac{c}{6a} + \frac{2b^2}{3ca} - \frac{b}{3a}, \tag{4.4}$$

where $a = \frac{1-t}{P(0)}$, $b = \frac{\Sigma}{P(0)}$ and $c = (108a^2 - 8b^3 + 12\sqrt{3}\sqrt{27a^2 - 4b^3}a)^{1/3}$.

4.1.3. $\Theta_V \to 0$ *and* $\Theta_D \sim 1$

If $\Theta_D \sim 1$, the simplifications of section 4.1.1 no longer hold. There is, for instance, no possible simplification for equations (2.16) and (2.18). Nevertheless, since $\Theta_V << 1$, we have:

$$P = 1 - t + \frac{\Sigma}{R} \tag{4.5}$$

which links the bubble pressure P to the radius R. On the other hand, considering that $M = PR^3$ and equation (2.16), we obtain the following differential equation for R:

$$\dot{R} = \left(\frac{3\rho_m}{\Theta_D} \left(r^2 \frac{\partial C}{\partial r} \right)_{r=R} + R^3 \right) \left(2\Sigma R + 3R^2(1-t) \right)^{-1}, \tag{4.6}$$

where the water concentration is obtained solving the advection-diffusion equation (2.18).

Numerically, we respectively compute M^{n+1} and C_i^{n+1} using the general numerical schemes for equations (3.2) and (3.6), then we apply relation $M = PR^3$ to compute P and finally from (4.5) we obtain R.

4.2. *Equilibrium regime:* $\Theta_V/\Theta_D \sim 1$

In this section we deal with those regimes in which the relaxation parameters Θ_V and Θ_D are of the same order of magnitude. More precisely, when both Θ_V and Θ_D go to zero, or to ∞, since otherwise no simplification is possible.

4.2.1. $\Theta_V \to 0$ *and* $\Theta_D \to 0$

This is an interesting situation because on the one hand computational time is very long and on the other hand it corresponds to the so-called equilibrium growth, which is a common situation in natural magmas: the bubble is always at its maximum possible radius. First notice that, since $\Theta_V << 1$, following the discussion of section 4.1.3, we have the simplification (4.5).

Next, let us consider $\Theta_D << 1$, then multiplying the water concentration equation (2.18) by Θ_D and simplifying, we have:

$$\frac{1}{r^2} \frac{\partial}{\partial r} \left(r^2 \frac{\partial C}{\partial r} \right) = 0,$$

for which the solution, taking into account the boundary conditions (2.19), reads:

$$C(r,t) = C(R,t) = C_i \sqrt{P}, \quad \forall\, r \in [R(t), S(t)], \tag{4.7}$$

Thus, we see that when Θ_D tends to zero, equation (2.16) is no longer valid to compute the water mass variation inside the bubble. Therefore, we consider the total mass conservation equation (2.14). Replacing C by (4.7) in (2.14) and recalling (2.13), we obtain

$$M = \rho_m S_0^3 (C_0 - C_i \sqrt{P}), \tag{4.8}$$

Now since $M = PR^3$, equation (4.8) is a second order equation in $X = \sqrt{P}$, which turns out to have one positive solution, namely

$$P = \left(\frac{-Y + \sqrt{Y(Y + 4R^3 C_0/C_i)}}{2R^3} \right)^2, \quad \text{where } Y = C_i \rho_m S_0^3. \tag{4.9}$$

Hence R and P (or M) are uniquely defined by combining (4.5) with (4.9) or (4.8) (which we have used in practice).

Notice that equation (4.8) allows to derive an expression for the porosity $\alpha = \alpha(t)$. Indeed, recall that the porosity is defined by $\alpha = R^3/S^3$, so that we have

$$R^3 = S_0^3 \frac{\alpha}{1-\alpha}.$$

Replacing M by PR^3 in (4.8) gives readily

$$P \frac{\alpha}{1-\alpha} = \rho_m \big(C_0 - C_i \sqrt{P}\big),$$

which in turns leads to

$$\alpha = \frac{\beta}{P+\beta}, \quad \text{where } \beta = \rho_m \left(C_0 - C_i \sqrt{P}\right). \tag{4.10}$$

Going back to dimensional quantities in (4.10), we get

$$\alpha_{dim} = \frac{\gamma}{M_w \hat{P} + \gamma}, \quad \text{where } \gamma = RT \hat{\rho_m} K_H \left(\sqrt{\hat{P}_0} - \sqrt{\hat{P}} \right), \tag{4.11}$$

which is equivalent to the most commonly used formula to calculate porosity in this regime (see e.g. Ref. 10). Nevertheless, we underline that in (4.11) it is accounted for the surface tensor term, since $\hat{P} = \hat{P}_a + 2\sigma/\hat{R}$, which is instead neglected in the usual one, in which $\hat{P} = \hat{P}_a$.

4.2.2. $\Theta_V \to \infty$ *and* $\Theta_D \to \infty$

In this situation, viscosity may be very large, yielding $\Theta_V >> 1$, and diffusivity very small, implying $\Theta_D >> 1$. Hence, following experimental evidence (see Ref. 7), we can imagine that the physical system is "fixed" or "frozen".

On the one hand, as discussed in section 4.1.1, the water mass in the bubble is constant, see equation (4.2). On the other hand, since $\Theta_V >> 1$, from equation (2.15) we also obtain $\dot{R} = 0$, that is:

$$R(t) = R(0) = 1. \tag{4.12}$$

Since both the mass M and the radius R are constant, the pressure P is explicitly determined by $M = PR^3$, and no numerical scheme is needed.

4.3. *Diffusive regime :* $\Theta_V/\Theta_D >> 1$

In this last section, we treat regimes which have the viscous Θ_V relaxation parameter larger than the diffusion one Θ_D. We have to differentiate three cases: when Θ_D is small and Θ_V is of order one or goes to infinity, and when Θ_D is of order one and Θ_V goes to infinity.

4.3.1. $\Theta_V \to \infty$ *and* $\Theta_D \sim 1$

As shown before, when $\Theta_V \to \infty$, we obtain equation (4.12). Hence, the bubble radius is constant in time, and recalling that $M = PR^3$, we have $\dot{M} = \dot{P}$, hence from (2.16) we get the following differential equation on P:

$$\dot{P} = \frac{3\rho_m}{\Theta_D} \left(r^2 \frac{\partial C}{\partial r} \right)_{r=R}, \tag{4.13}$$

with C solution of (2.18).

Numerically, the radius R is constant, and the pressure P is computed using the numerical scheme of section 3.

4.3.2. $\Theta_V \to \infty$ *and* $\Theta_D \to 0$

Considering the discussion of sections 4.2.2 and 4.2.1, both simplifications (4.12) and (4.9) hold. From (4.12), the bubble radius is constant, $R = 1$, so that the bubble pressure is also constant, and is explicitly obtained by simplifying equation (4.9):

$$P = \left(\frac{-Y + \sqrt{Y(Y + 4C_0/C_i)}}{2} \right), \quad Y = C_i \rho_m S_0^3. \tag{4.14}$$

4.3.3. $\Theta_V \sim 1$ *and* $\Theta_D \to 0$

Since $\Theta_V \sim 1$, there is no possible simplification for equation (2.15). On the other hand, from section 4.2.1, the bubble pressure is computed by (4.9).

In this case, the radius R must be computed using the numerical scheme of section 3, while the pressure P is explicitly given by (4.9).

5. Numerical results

We performed some numerical tests based on the schemes described in sections 3 and 4. In this section we compare first the numerical results obtained using the general scheme of section 3 to those obtained with the numerical approximation of the simplified schemes of section 4. This is followed by a comparison between the behavior of our numerical results and experimental data described in Burgisser *et al.*[2]

Le us first discuss the dependence of our results on the number of discretization points N with respect to the radial variable r. As announced previously, various numerical tests show that a small number of points is sufficient in order to well

capture the behavior of the discrete flux F_0^n on the bubble border. The relative errors of the curves for the bubble radius R, bubble pressure P, and porosity α with respect to the reference ones with $N = 2500$, are of order 10^{-3} for $N = 50$ and of order 10^{-4} for $N = 250$, respectively. We therefore choose $N = 50$ in all the following computations.

In figure 1 we show the evolution of the concentration function $C(t, r)$ computed solving the general scheme with $\Theta_V = 0.000236$ and $\Theta_D = 5.28929$. Bubble size evolution is sketched as grey circles of increasing radius R. We clearly see the mesh refinement near the bubble wall (the grey circle portion) when the concentration function becomes stiffer.

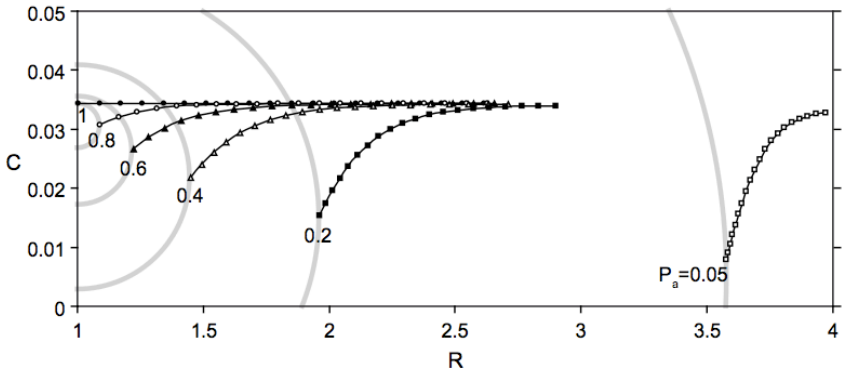

Fig. 1. Bubble growth and gas concentration function in the influence region.

5.1. *Numerical convergence*

We show now through a few selected examples the numerical convergence of the global numerical scheme defined in section 3 towards the simplified limit cases discussed in section 4. Convergence is determined by fixing either the value of Θ_V or Θ_D and varying the other one. This crossed method yields to the Θ_V and Θ_D orders of magnitude for which the system changes regime. We can see in table 2 that for $\Theta_V < 10^{-5}$ and $\Theta_D < 10^{-3}$ we have the so called equilibrium regime, whereas for $\Theta_V > 10^1$ and for each Θ_D the bubble radius is constant. These results suggest that the simplified limit cases are sufficient for a good description of the physical system. Their use significantly reduces computation time.

In figure 2 we show the convergence for the bubble radius towards selected limit cases. On the left, we plot the bubble radius evolution with respect to the ambient pressure P_a (we recall that ambient pressure linearly decreases in time as : $1 - t$), fixing $\Theta_D = 0.1$ and varying Θ_V from 10^{-5} to 10^1, together with the radius computed as explained in 4.1.3 or just defined as the constant 1, as justified in

4.3.1. On the right, we plot the bubble radius evolution with respect to time, fixing $\Theta_V = 0.1$ and varying Θ_D from 10^{-3} to 10^3, together with the radius obtained as explained in 4.1.1 and 4.3.3. In both cases we can observe the transition of the general unsimplified regime (the middle case in table 2) from one simple growth regime to the next.

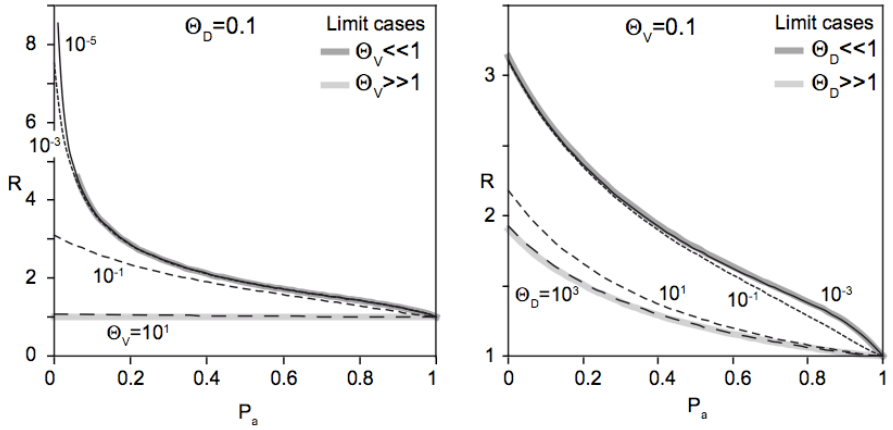

Fig. 2. Bubble radius evolution and convergence. Left: convergence towards the limit cases 4.1.3 and 4.3.1. Right: convergence towards the limit case 4.1.1 and 4.3.3.

5.2. *Experiments vs. numeric*

Controlled decompression experiments on high temperature magmas are able to produce gas bubbles. By varying the end pressure, data on bubble size and porosity have been retrieved for different initial condition such as magma viscosity, temperature, decompression rate, etc. In this work we illustrate how comparisons between such experimental data and model outputs can be carried out. Let us first present here the experimental framework used by Burgisser *et al.*[2] Samples of viscous magma are saturated in water and maintained under pressure for about 5 days for the water to homogeneously dissolved into the magma. Then an instantaneous decompression gives rise to bubble nucleation. After waiting for a few minutes that these initial, small bubble reach their equilibrium sizes, a linear decompression is applied until a final pressure where samples are quenched by a sudden cooling to ambient temperature. The cold samples are then sliced and analysed to obtain bubble sizes and porosity. One experiment quenched just after the sudden decompression that nucleates the bubbles gives the initial conditions for our model.

The physical values used and measured during the experiments are the following: the initial radius $R_i = 17.5 \cdot 10^{-6}$, the diffusion coefficient $D_i = 5.79 \cdot 10^{-12}$, the initial concentration $C_0 = 3.44 \cdot 10^{-2}$, the initial pressure $P_i = 10^8$, the surface

tension $\sigma = 0.1$, the viscosity $\eta_i = 5.9 \cdot 10^{-4}$, the magma density $\rho_m = 2400$, the gas porosity density ρ_i being calculated by the perfect gas law (2.1), the temperature $T = 825$, and the decompression rate $\Delta P = 10^{-5}$. We tested two different experimental series. In the first series, bubbles growth was only due to gas expansion and water diffusion form the magma. In the second series, bubbles growth was also due to coalescence processes. The porosity evolution of both series is comparable but the evolution of bubble size differ.

In figure 3 we show the evolution of the porosity α and of the radius R with respect to the ambient pressure P_a. On the left graph are represented three numerical results for different viscosity calculation and initial porosities along with the experimental results obtained in Ref. 2 (triangles). The run represented by the grey line had a constant viscosity η, whereas the black line and the dashed line had variable viscosity η_{eff} computed applying the formula given in Ref. 9 and 11. We remark that considering a variable viscosity η_{eff} instead of a constant one has an impact on the numerical result only when the ambient pressure becomes very small because the grey and the black curves diverge only when $P_a < 0.1$. The dashed line is a numerical result computed starting from the porosity measured on the experiment quenched just after the sudden decompression. The other two runs use the equilibrium state in Section 4.2.1, which predicts a porosity of 0.0779 instead of 0.056. We note that the experimental points fit better the dashed line at high P_a and are closer to the two other curves at low P_a. This lead us to conclude that during the first phase of the experiments the time waited between nucleation and the beginning of the decompression was not enough to reach the equilibrium.

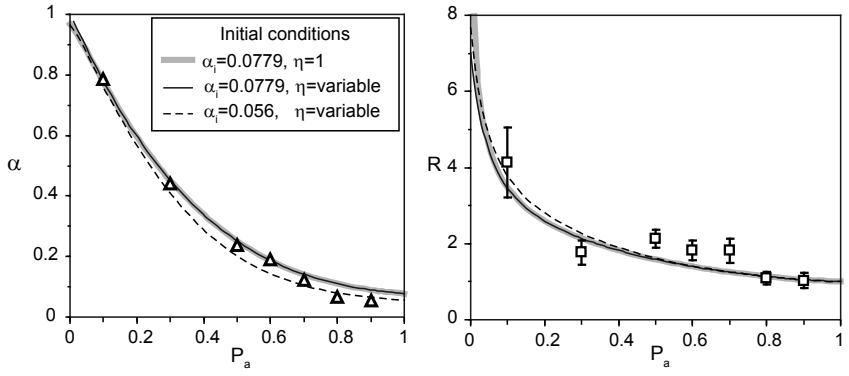

Fig. 3. Porosity α (on the left) and radius R (on the right) with respect to ambient pressure P_a: effect of a variable viscosity η_{eff}.

The right graph shows the numerical radii R as a function of the ambient pressure P_a for the same three numerical runs (on the left). Experimental results are

now represented with square points centred on the median value of the experimental radii together with a standard deviation representing the spread of measured bubble radii. We note that the three runs are very similar, regardless of initial conditions, and that the fit between experiments and numerical results is worst for radius than porosity. The larger misalignment of experimental radii compared to that of porosity is explained by the fact that each experimental point in figure 3 is a full decompression run starting from $P_a = 1$. As a result, bubble nucleation dynamics occurring during the initial decompression step is only approximately similar from one experiment to the next.

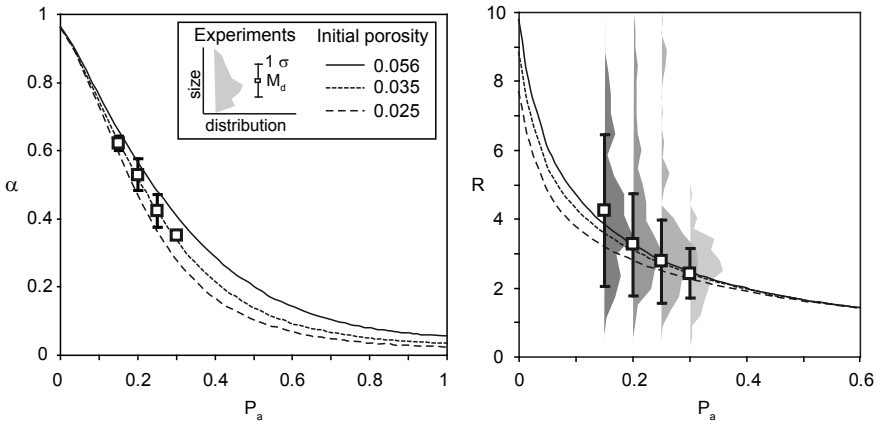

Fig. 4. Bubble radius R with respect to ambient pressure P_a: mono-disperse vs. poly-disperse.

In figure 4 we compare the experimental results obtained in Ref. 2 when bubble coalescence occurs with our numerical results with variable viscosity for three different initial porosities. The left graph, which displays the evolution of porosity with ambient pressure, indicates that this experimental series is best reproduced numerically by starting from a initial porosity of 0.035. This is lower than the best fit value of the other series. A tentative explanation of this situation is a even shorter pause between bubble nucleation and the start of the decompression. We plotted on the right graph, which shows the evolution of R with ambient pressure, distribution histograms of measured bubble radii. The three computed bubble radius R all fit the experimental measurements within a standard deviation, but, considering the large spread of bubble sizes, it is not possible to choose which numerical results has the better fit. As discussed in Ref. 2, this layout is due to the poly-disperse nature of bubble growth in the experiments, which was caused by bubble coalescence. Hence, in order to produce more accurate results that resolve the spread in bubble sizes, one should consider poly-disperse modelling of the bubbles population.

Furthers comparisons with other experimental results is under investigation and will be exposed in a future work. We simply underline herein that our numerical code has a satisfactory behavior when confronted to various experimental works, and that it is sufficiently accurate to point experimental shortcomings as long as poly-disperse processes do not dominate bubble growth.

6. Conclusions

In the present paper, we have proposed and applied a numerical scheme for the approximation and simulation of the solution of a non-linear system of differential equations coupled with an advection diffusion equation, popularised in the volcanology literature by Prussevitch *et al.*[13] and Lensky *et al.*[11] Our goals were twofold: give a conservative discretization of the system and study the asymptotic limits when the two relaxation parameters Θ_V and Θ_D went to 0 or ∞.

In the recent years (see for example Ref. 5 and the reference therein), the numerical approach to solve the model governed by equations (2.15)-(2.16)-(2.18) is based on the one proposed in Ref. 15: the transport term in the advection-diffusion equation is simplified by the means of a change of variable at the continuum level, leading to a kind of heat equation (the diffusion term is not standard). Nevertheless, with the method proposed in Ref. 13, a large number N of discretisation points in the radial direction is greatly reduced by the means of a variable mesh size. This size is controlled by an empirically defined parameter that ensures the conservation of water mass and that precisely captures the behavior of the flux on the bubble border. With our approach, a small number of points, $N = 50$, also guarantees precise results, but the mesh size is automatically defined. In fact, the discrete flux on the bubble border is defined in such a way that the numerical scheme preserves water mass (see Proposition 3.1). There is thus no need to adjust an empirical parameter to ensure scheme accuracy.

Concerning the asymptotic behavior of the coupled system of equations, we have analytically deduced the different simplified models in the three regimes: viscous, when $\Theta_V/\Theta_D << 1$, diffusive, when $\Theta_V/\Theta_D >> 1$, and in the equilibrium one, when $\Theta_V/\Theta_D \sim 1$. In particular, when both Θ_V and Θ_D go to 0, we retrieve the equilibrium state of the problem. We have numerically shown the convergence of the scheme towards the solutions of the three regimes when varying the relaxation parameters. We also determined numerically the boundaries between the various regimes.

Finally we compare our numerical results with data obtained from decompression experiments of natural magmas. This validation of the code gives also a feedback on the quality of experimental results. In particular, we show that, unlike originally assumed by the authors, decompressions in Ref. 2 started while bubbles were still growing, i.e. equilibrium was not reached. Finally, it appears that the simplified mono-disperse framework is not accurate enough (see figure 4) to capture spreading bubble size distributions such as those produced by bubble coalescence.

We thus infer that an extension of the physical model to include a poly-disperse description for the bubbles population is a worthy pursuit.

Acknowledgment

This work was partially founded by the ERC-starting grant DEMONS (n. 202844) under the European FP7.

References

1. A. Arefmanesh and S.G. Advani, Diffusion-induced growth of a gas bubble in a viscoelastic fluid, *Rheol. Acta* **30** (1991) 274–283.
2. A. Burgisser and J.E. Gardner, Experimental constraints on degassing and permeability in volcanic conduit flow, *Bull. Volcanol.* **67** (2005) 42–56.
3. T. Beechem, K. Lafdi and A. Elgafy, Bubble growth mechanism in carbon foams, *Carbon* **43** (2005) 1055–1064.
4. J.D. Blower, H.M. Mader and S.D.R. Wilson, Coupling of viscous and diffusive controls on bubble growth during explosive volcanic eruptions, *Earth and Plan. Sci. Letters* **193** (2001) 47–56.
5. B. Chouet, P. Dawson and M. Nakano, Dynamics of diffusive bubble growth and pressure recovery in a bubbly rhyolitic melt embedded in an elastic solid, *J. Geophys. Res.* **111** (2006) B07310.
6. J.E. Gardner, The impact of pre-existing gas on the ascent of explosively erupted magma, *Bull. Volcanol.* **71** (2009) 835–844.
7. J.E. Gardner, M. Hilton and M.R. Carroll, Bubble growth in highly viscous silicate melts during continuous decompression from high pressure, *Geoch. et Cosmoch. Acta* **64** (2000) 1473–1483.
8. I. L'Heureux, A new model of volatile bubble growth in a magmatic system: Isobaric case, *J. Geophys. Res.* **112** (2007) B12208
9. K-U. Hess and D.B. Dingwell, Viscosities of hydrous leucogranitic melts: a non-Arrhenian model, *Amer. Mineral.* **81** (1996) 1297–1300.
10. C. Jaupart and C. Allegre, Gas content, eruption rate and instabilities of eruption regime in silicic volcanoes, *Earth and Plan. Sci. Letters* **102** (1991) 413–429.
11. N.G. Lensky, O. Navon and V. Lyakhovsky, Bubble growth during decompression of magma : experimental and theorical investigation, *J. Volc. Geoth. Res.* **129** (2004) 7–22.
12. A.A. Proussevitch and D.L. Sahagian, Dynamics and energetics of bubble growth in magmas: Analytical formulation and numerical modeling, *J. Geophys. Res.* **103** (1998) 18223–18251.
13. A.A. Proussevitch, D.L. Sahagian and A.T. Anderson, Dynamics of diffusive bubble growth in magma: isothermal case, *J. Geophys. Res.* **98** (1993) 22283–22307.
14. G. Rosebrock, A. Elgafy, T. Beechem and K. Lafdi, Study of the growth and motion of graphitic foam bubbles, *Carbon* **43** (2005) 3075–3087.
15. L.E. Scriven, On the dynamics of phase growth, *Chem. Eng. Sci.* **10** (1959) 1–13.
16. A. Toramaru, Numerical study of nucleation and growth of bubbles in viscous magmas, *J. Geophys. Res.* **100** (1995) 1913–1931.
17. J.S. Vrentas and C.M. Vrentas, Slow bubble growth and dissolution in a viscoelastic fluid, *J. Appl. Polymer Sc.* **67** (1998) 2093–2103.
18. S.W.J. Welch, Direct simulation of vapor bubble growth, *Int. J. Heat and Mass Transfer* **41** (1998) 1655–1666.